Published in final edited form as:
Mol Cancer Res. 2014 April ; 12(4): 607–621. doi:10.1158/1541-7786.MCR-13-0469.

CAF-secreted Annexin A1 Induces Prostate Cancer Cells to Gain Stem Cell-like Features

Lauren A. Geary[1], **Kevin A. Nash**[1], **Helty Adisetiyo**[2], **Mengmeng Liang**[1], **Chun-Peng Liao**[3], **Joseph H. Jeong**[4], **Ebrahim Zandi**[5], and **Pradip Roy-Burman**[1,2,6]

[1]University of Southern California, Keck School of Medicine, Department of Pathology, Los Angeles, CA 90033, USA

[2]University of Southern California, Keck School of Medicine, Department of Biochemistry and Molecular Biology, Los Angeles, CA 90033, USA

[3]University of Southern California, Keck School of Medicine, Center for Applied Molecular Medicine, Los Angeles, CA 90033, USA

[4]Medical College of Wisconsin, Department of Dermatology, Milwaukee, WI 53226, USA

[5]University of Southern California, Keck School of Medicine, Department of Molecular Microbiology and Immunology, Los Angeles, CA 90033, USA

Abstract

Annexin A1 (AnxA1), a phospholipid-binding protein and regulator of glucocorticoid-induced inflammatory signaling, has implications in cancer. Here, a role for AnxA1 in prostate adenocarcinoma was determined using primary cultures and a tumor cell line (cE1), all derived from the conditional *Pten* deletion mouse model of prostate cancer. AnxA1 secretion by prostate-derived cancer-associated fibroblasts (CAFs) was significantly higher than by normal prostate fibroblasts (NPFs). Prostate tumor cells were sorted to enrich for epithelial subpopulations based on non-hematopoietic lineage, high SCA-1, and high or medium levels of CD49f. Compared to controls, AnxA1 enhanced stem cell-like properties in high- and medium-expression subpopulations of sorted cE1 and primary cells: *in vitro*, through formation of greater number of spheroids with increased complexity; and *in vivo*, through generation of more, larger and histologically complex glandular structures, along with increased expression of p63, a basal/progenitor marker. The differentiated medium-expression subpopulations from cE1 and primary cells were most susceptible to gain stem cell-like properties as shown by increased spheroid and glandular formation. Further supporting this increased plasticity, AnxA1 was shown to regulate epithelial-to-mesenchymal transition (EMT) in cE1 cells. These results suggest that CAF-secreted AnxA1 contributes to tumor stem cell dynamics via two separate but complementary pathways:

[6]**To whom correspondence should be addressed:** Pradip Roy-Burman, University of Southern California, Keck School of Medicine, Department of Pathology, 2011 Zonal Avenue, HMR 210B, Los Angeles, CA 90033, Tel: 323-442-1184, Fax: 323-442-3049, royburma@usc.edu.

Conflicts of Interest: The authors declare no conflicts of interest

Implications

AnxA1 participates in a paradigm in which malignant prostate epithelial cells that are not cancer stem cells are induced to gain cancer stem cell-like properties.

induction of a de-differentiation process leading to generation of stem-like cells from a subpopulation of cancer epithelial cells, and stimulation of proliferation and differentiation of the cancer stem-like cells.

Keywords

annexin a1; prostate cancer; cancer stem cells; EMT; adenocarcinoma

Introduction

Annexins comprise a family of proteins that bind to specific phospholipids in a calcium-dependent manner [1, 2]. The calcium-binding and phospholipid-binding sequences of annexins are encoded for in the conserved C-terminus (40–60% homology), whereas an N-terminus of varying length and sequence is unique to each family member and confers the specific biological activity [3]. Annexin A1, a 37kDa protein, the first characterized member of the family, was originally reported for its anti-phospholipase activity after glucocorticoid induction [4, 5]. Subsequent studies showed that both recombinant AnxA1 and AnxA1-derived N-terminal peptides possess a wide range of anti-inflammatory properties [6–8]. In addition to the regulatory region, the N-terminus also contains the sites for phosphorylation [3]. Various signal transducing kinases, such as EGF receptor tyrosine kinase, platelet-derived growth factor receptor kinase, hepatocyte growth factor receptor kinase, TRPM7 channel kinase and protein kinase C (PKC) are known to phosphorylate AnxA1 and contribute to its biological function [9, 10].

AnxA1 does not possess a recognized signal sequence for targeting to the endoplasmic reticulum [11]. It appears to follow a cell-specific novel manner of secretion [12]. In neutrophils, gelatinase granules store high levels (>60%) of cytoplasmic AnxA1 for extrusion upon activation [13]. Cells that do not store AnxA1 in granules display another distinct secretory pathway. In macrophages and pituitary folliculo-stellate cells, AnxA1 is exported by the ATP-binding cassette A1 (ABC-A1) transporter system or ATP-sensitive K^+ channels [14–17]. In both leukocytes and pituitary cells phosphorylation on Ser^{27} is necessary for protein export and secretion. This action is directed by Ca^{2+}-dependent isoforms of PKC, and subsequent translocation of the $serine^{27}$-phosphorylated species of AnxA1 to the plasma membrane occurs at specific lipid domains that allow for secretion [18–20]. Extracellular Ser^{27}-AnxA1 undergoes a conformational change in the presence of ≥ 1 mM Ca^{2+} causing exposure of the N-terminal domain from inside the pore created by the four repeated motifs of the core domain and, thereby, binding to its receptor [19, 21]. Binding of AnxA1 to the receptor activates downstream signaling via phosphorylation of the mitogen-activated protein kinase (MAPK) Erk1/2 [22–24].

Through its specific N-terminal sequence, AnxA1 directly interacts with a family of G-protein coupled receptors, the formyl peptide receptors (FPRs), which includes FPR1, FPR2 (also known as ALXR) and FPR3 in humans and Fpr1 and Fpr-related proteins (Fpr-rs) 1–7 in mouse [25, 26]. Endogenous and recombinant full-length AnxA1 specifically bind to FPR2/ALXR and murine Fpr-rs1 (approximately 30% activity has been selectively

demonstrated for Fpr1), whereas the bioactive N-terminal-derived peptide comprised of amino acids 2-26, Ac2-26, was shown to activate all members of the human FPR family and the murine Fpr1 and Fpr-rs1, and may additionally activate Fpr-rs2 [6, 12, 25, 27].

Regarding tissue distribution, AnxA1 is found in high abundance in lung, bone marrow, intestine, lymphatic tissue and reproductive tracts, and interestingly, with highest concentration in the seminal fluid of the prostate (150 μg/ml) [11]. It is also found to have differential expression in certain cancers [28]. In prostate cancers, AnxA1 loss of expression from the ductal epithelial cells was reported [29–33]. Prostatic stromal cells also display expression of AnxA1 [11]. In ductal carcinoma *in situ* and invasive carcinoma breast tumors, stromal AnxA1 expression was positively correlated with infiltration of both epithelial and stromal cells [34].

We previously described evidence that cancer-associated fibroblasts (CAFs), derived from the stromal compartment of prostate tumors, secrete factors that enhance both the stemness and growth potentials of cancer stem cells (CSCs) from the primary prostate tumor [35]. We used the conditional *Pten* deletion with activated luciferase reporter (*cPten*$^{-/-}$*L*) mouse model of prostatic adenocarcinoma [36, 37]. Here, we identified AnxA1 as one of the pertinent secreted factors. AnxA1 treatment of a prostate cancer cell line from the mouse model led to up-regulation of epithelial-to-mesenchymal (EMT) transcription factors as well as pluripotency transcription factors *in vitro*. Primary epithelial tumor cells or cells of the cell line treated with AnxA1 displayed enhanced glandular structure formation and basal/progenitor marker p63 expression *in vivo*, compared to controls. Treatment with AnxA1 *in vitro* and *in vivo* is associated with pErk1/2 activation. Together, these findings indicated that AnxA1 might be involved in *de novo* generation of CSCs from cancer cells as well as maintenance of the CSC population.

Materials and Methods

Animals

The conditional *Pten* deletion mouse model with luciferase reporter (*cPten*$^{-/-}$*L*) used in the current work was described previously [36]. For renal tissue grafting, non-obese diabetic severe-combined immunodeficient (NOD.SCID) mice, purchased from National Cancer Institute (Frederick, MD), were used. All protocols were approved by the Animal Care Committee of the University of Southern California.

Isolation of murine cells and sorting

Urogenital sinus mesenchyme (UGSM) [38], normal prostate fibroblasts (NPFs) and CAFs [39] were isolated following published procedures. The generation of the cE1 prostate cancer cell line from the mouse model was described [40]. Preparation of primary cultures of epithelial cells from single cell suspensions of minced prostate tumors from *cPten*$^{-/-}$*L* mice [36], cell staining and isolation by fluorescence-activated cell sorting (FACS), with exception of fluorophores used (see Supplementary Materials and Methods), were described before [35].

Cell culture and assays for spheroid formation

Growth of epithelial cells in Matrigel has been described [35]. Cells were co-cultured with fibroblasts or treated with conditioned media as indicated in the results. For co-culture experiments, epithelial cells were embedded in Matrigel, and fibroblasts were grown in chamber inserts at 10:1 fibroblast to epithelial cells. LNCaP human prostate cancer cells [American Type Culture Collection (ATCC)], and PC3 (ATCC), were plated on Matrigel pre-coated wells. For detailed cell culture conditions, see Supplementary Materials and Methods.

Conditioned media and AnxA1 ligands

CAF and NPF conditioned media (CM) were prepared by 24 hour incubation of serum free DMEM/5 μg/ml insulin with confluent stromal cultures. Collected medium was centrifuged at 300 × g for 5 minutes to remove contaminants, normalized by protein quantification using Bradford reagent (Bio-Rad) in a Benchmark Plus Microplate Spectrophotometer (Bio-Rad) and also compared to number of fibroblast cells per plate, counted at time of collection. After concentration using Amicon Ultra-15 3K Centrifugal Filter Units (Millipore), CM was used to treat epithelial cells at 0.04 mg/ml or ratio of 10:1 fibroblast to epithelial cells. Ammonium sulfate CM fractions were prepared following a published procedure [41]. Pelleted proteins were solubilized in 1× PBS and dialyzed overnight, followed by centrifugal concentration.

Murine recombinant AnxA1 protein was produced as an N-terminal 6×His tag fusion protein. Full-length mouse AnxA1 cDNA (Invitrogen) was subcloned into pET/TOPO-D vector in BL21 Star™ (DE3; Invitrogen) bacteria. Protein expression was induced by 1 mM isopropyl-thio-galactoside. Fusion protein was extracted using 6×His Fusion Protein Purification Kit and purified using Pierce High Capacity Endotoxin Removal Spin Columns, both from Thermo Scientific, followed by centrifugal concentration. Peptide Ac2-26 (acetyl-AMVSEFLKQAWFIENEEQEYVQTVK-OH trifluoroacetate salt; M_r 3089) was purchased from Bachem. Purity was more than 94% as assessed by high performance liquid chromatography (data supplied by manufacturer).

Renal grafting

Murine cell line and primary epithelial cells were treated with vehicle control, CAF CM, peptide Ac2-26 or recombinant AnxA1 for 14 days prior to being passaged for transplantation. During passaging, cells did not receive additional treatment. As published [42], epithelial cells (10^4) were mixed with stromal cells (10^4) in 70 μL neutralized rat tail collagen type I (BD Biosciences) before transplanting under the renal capsule of 8- to 12-week-old male NOD.SCID mice [35]. See Supplementary Materials and Methods for full details.

Immunostaining and western blots

Preparation of spheroids and renal tissues for immunostainings was as previously described [35, 36]. Primary antibodies for immunostains, western blots and neutralizing antibody against N-terminal residues of AnxA1, dilutions, and manufacturers are listed in Supplementary Table S1. Photomicrographs were captured with Spot Advanced software

(Spot™ Imaging Solutions) and quantified with ImageJ software (National Institutes of Health). Immunoblots were captured and quantified with Image Lab™ software (Bio-Rad). For western blot analysis, whole cell lysates were prepared by addition of RIPA buffer (Sigma) with proteinase inhibitor (Roche) and phosphatase inhibitor cocktails II and III (Sigma) at a 1× final concentration (manufacturer's protocols).

PCR analyses

Extraction of total cellular RNA, reverse transcription reaction and quantitative real-time PCR were performed and analyzed as described [35]. Primer sets are listed in Supplementary Table S2.

Statistical analysis

All data are presented as means ± SD. qRT-PCR data are shown as means ± SD of repeat analyses. Differences between individual groups were analyzed by paired *t* test or χ^2, as appropriate, using Excel (Microsoft® Office) and InStat (GraphPad Software, Inc.©) software. *P* values of < 0.05 were considered to be statistically significant.

Results

Effect of CAFs on Prostate Cancer Cells

We previously demonstrated that CAFs could stimulate the proliferation and tumorigenicity of prostate CSCs via a paracrine/juxtacrine interaction *in vivo* [35]. Here we constituted a test system comprised of a prostate tumor cell line and primary cultures of CAF or normal prostate fibroblasts (NPF) [39], all from the *cPten*$^{-/-}$*L* mouse model. The tumor cell line, cE1, which was derived from a castration-resistant prostate cancer (CRPC) of the same model [36] was described earlier [40]. We observed that co-culture of NPF and CAF had a differential effect on the epithelial cells. The cE1 cells co-cultured with CAF displayed morphological changes akin to EMT as compared to cE1 cells either grown under control conditions without co-culture or cE1 cells co-cultured with NPF (Fig. 1A).

Considering the presence of phenotypic heterogeneity, even in a cell line, cE1 cells were subjected to FACS to enrich for subpopulations of putative tumor-initiating/progenitor cells based on cell surface expression levels of mouse stem cell antigen-1 (SCA-1) and laminin receptor α6 (CD49f). Our rationale for this analysis was based upon a recent body of published work whereby prostate cancer putative stem cells have been described. The hematopoietic Lineage (Lin) negative (CD31/CD45/TER119)$^-$/SCA-1$^+$/CD49f$^+$ (LSC) phenotype within prostatic tissue cells was determined to contain cells with properties of self-renewal and differentiation [43, 44]. Further enrichment for Lin$^-$/SCA-1^{hi}/CD49f^{hi} (LSC^{hi}) cells based on high expression levels of SCA-1 and CD49f, led to increased capability for generation of prostate glandular structures *in vivo* [35]. Subpopulations of cE1 cells displaying high, medium or no expression of SCA-1 and CD49f (SC^{hi}, SC^{med} or SC^{none}, respectively) were recovered (Fig. 1B). Lineage markers were not necessary for selection by FACS for cE1 cells because contaminating non-epithelial cell types were removed during derivation of the cell line [40].

We described the formation of spheroids after co-culture of $Lin^{-}SCA\text{-}1^{+}$ (LS) cells from primary *cPten*$^{-/-}$*L* tumors in a Matrigel matrix with either NPFs or CAFs that were grown in inserts [35]. Spheroids produced in co-culture with CAFs were larger in size and were composed of multiple basal and luminal cell layers as opposed to those spheroids generated with NPFs or without stromal cells [35]. After further fractionation of the LS cells into LSC^{hi} and $Lin^{-}/SCA\text{-}1^{hi}/CD49f^{med}$ (LSC^{med}), we found that spheroid-forming cells largely segregated with the LSC^{hi} subpopulation [35]. We applied a similar approach to 3-D culture of the tumor cell line derived SC^{hi} and SC^{med} cell fractions. SC^{hi} and SC^{med} contained cells that showed spheroid-forming ability, and the growth of the spheroids from both SC^{hi} and SC^{med} were stimulated by conditioned medium (CM) collected from CAF. After CAF CM stimulation, the spheroids formed from SC^{med} appeared to contain increased number of CK5 and CK8 double positive cells, possibly indicative of more transit-amplifying cells, relative to those from the SC^{hi} cells (Fig. 1C).

The results of qRT-PCR analyses of SC^{hi} and SC^{med} indicated some characteristic differences between these two subpopulations. As shown in Fig. 1D, SC^{hi} cells grown under control culture conditions displayed significantly higher basal expression levels of pluripotency transcription factors Oct4 ($P < 0.01$), Nanog ($P < 0.001$) and Sox2 ($P < 0.001$), and transcription factor Snail ($P < 0.01$) as compared to SC^{med} cells. Encouraged by these differences in basal levels, we then proceeded to determine the expression levels of Oct4, Sox2, Nanog, and EMT transcription factors Snail, Slug and Twist, and epithelial marker E-cadherin, and mesenchymal markers N-cadherin and Vimentin in SC^{hi}, SC^{med} and SC^{none} cells following exposure to CM from either CAF or NPF cultures. We noted extensive EMT-like phenotypic changes induced in SC^{med} cells by CM from CAFs and much less by that from NPFs (Supplementary Fig. S1A). Correspondingly, EMT'ed SC^{med} cells displayed a significant up-regulation of Oct4 ($P < 0.05$), Sox2 ($P < 0.001$), Snail ($P < 0.001$), Slug ($P < 0.01$), Twist ($P < 0.01$), N-cadherin ($P < 0.001$), Vimentin ($P < 0.05$) and significant decrease in E-cadherin ($P < 0.01$) as compared to SC^{hi} and SC^{none}, and up-regulation of Nanog ($P < 0.001$) as compared to SC^{hi} (Fig. 1E). These changes were tested over a 14 day period, wherein expression levels of these transcription factors and markers significantly increased in SC^{med} cells from day 7 to day 14 time points (Fig. 1F).

On the basis of these findings, we inferred that while SC^{hi} did display certain molecular characteristics of stem/progenitor cells, such as spheroid-formation capacity, SC^{med} cells appeared to be enriched with a tumor cell fraction that was especially susceptible to CAF-induced EMT. More importantly, the factors responsible for induction of this biological effect appeared to be contained within the conditioned medium prepared from CAF, indicating the presence of paracrine-acting secreted molecules.

A Search for Responsible CAF Factors Identifies AnxA1

To identify secreted factor(s) from the CAFs that are capable of inducing EMT and possibly contributing toward an *EMT-CSC* lineage, we decided to use fractionation techniques. Proteins from both NPF and CAF CM were salted out into five fractions following ammonium sulfate (AS) precipitation: 20%, 30%, 40%, 50% and 60%. Increased EMT-like morphology and gene expression level changes consistent with previous experiments were

seen when SC^{med} cells were exposed to CAF CM AS fractions, particularly at the 30%–40% AS cut (Supplementary Fig. S2). Silver stain visualization of the proteins after fractionation of NPF and CAF CM presented detectable levels of a dark band in both CAF CM and CAF CM fractions, but which appeared weak or absent in the NPF CM and NPF CM fractions. We selected this band as a potential candidate for mass spectrometry, an analysis that pointed to the phospholipid binding protein, AnxA1 (Fig. 2A, Supplementary Table S3). Western blot using an antibody against AnxA1 confirmed its abundance in the CAF CM fractions as compared to the NPF CM fractions (Fig. 2B).

Phosphorylation of AnxA1 on a specific serine residue (S^{27}) by protein kinase C (PKC) has been extensively reported to be necessary for extracellular secretion of the protein [18–20]. The presence of phospho-serine within the context of the specific amino acid recognition motif necessary for PKC mediated serine phosphorylation was assayed by western blot in CAF and NPF cultures. Multiple CAF cultures were shown to possess variably higher protein expression levels of phospho-Ser^{27}-AnxA1 than NPF cultures, in addition to generally higher total abundance of AnxA1 (Fig. 2C). CAF derived from larger tumors (cells recovered ≥ 20 million) produced four-fold more phospho-Ser^{27}-AnxA1 than smaller tumors (< 10 million cells), after normalization to protein mass (g). Analysis of phospho-Ser^{27}-AnxA1 relative to tumor size gave a linear regression with a correlation coefficient (R^2) of 0.9914 ($y = 4.1298x – 7.9487$, n=6). Known protein phosphorylators of AnxA1 were also assayed for up-regulation in CAFs versus NPFs. Transcriptional expression levels of *Pten*, *Trpm7* and selected *PKC* subtypes, revealed that *PKCδ* is significantly up-regulated in CAFs ($P < 0.01$; Fig. 2D).

Effect of AnxA1 on cE1 Cells *in vitro*

Neutralizing antibody (nAb) specific to the N-terminal portion of AnxA1 was incubated with cE1 cells treated with AnxA1 enriched fractions of CAF CM. Treatment with AnxA1 nAb showed a dose-dependent decrease in the number of spheroids greater than 50 microns ($P < 0.01$ at 5 μg/ml; $P < 0.001$ at highest dose, 20 μg/ml; Supplementary Fig. S3A). Similarly, exposure of cE1 cells to AnxA1 nAb at the lowest dose, 5 μg/ml, and in the presence of CAF CM led to a significant decrease in spheroid number in both SC^{hi} and SC^{med} cells grown in 3-D cultures ($P < 0.01$ and $P < 0.05$, respectively). These results indicated that the increased ability of cE1 cells to form spheroids in the presence of CAF CM could be negated by addition of the AnxA1 nAb (Fig. 3A). In further support of the ability of AnxA1 nAb to repress spheroid proliferation and EMT-like properties of AnxA1 treated cells, total cE1 cells were allowed to grow in Matrigel for 14 days in the presence of CAF CM, AS-enriched CAF CM fractions, or N-terminal mimetic peptide (Ac2-26) with, or without, addition of AnxA1 nAb. Addition of AnxA1 nAb to cE1 cells grown in the presence of CAF CM, AS-enriched CAF CM fractions, or Ac2-26 led to reduced expression of Snail, Slug, Twist and Oct4, indicating the importance of this protein in promoting EMT and certain features of stemness (Fig. 3B). Consistently, Snail and Oct4 expression was significantly upregulated after treatment with CAF CM, AS-enriched CAF CM fractions and Ac2-26. Twist upregulation was found to be significant after treatment with AS-enriched CAF CM fractions and Ac2-26. Pronounced and significant decrease in expression of Snail, Twist and Oct4 was consistently observed in cells exposed to AnxA1 nAb in the presence of

CAF CM, AS-enriched CAF CM fractions and Ac2-26, suggesting possible specificity of AnxA1 predominantly upon Snail, Twist and Oct4 dependent pathways (see *P* values in Fig. 3B).

Recent analyses have established that downstream signaling from interaction of soluble AnxA1 with its receptor, FPR2/ALXR in human and Fpr-rs1 in mouse, involves activation of phosphorylation of MAPK Erk1/2 (pErk1/2). Both mimetic and full-length proteins are able to bind to the receptor [27]. Up to 30% activity via Fpr1 was described [6]. We examined the expression of all three murine receptors hypothesized to be orthologous to human FPR1 and FPR2/ALXR in cE1 cells. Fpr-rs1 was found to be the most abundantly expressed, showing two-fold more prevalence over Fpr1 and Fpr-rs2 (Supplementary Fig. S3B).

Recently a basal-like breast cancer model was used to evaluate the effect of AnxA1 in the promotion of EMT and metastasis. In that study AnxA1 contributed to EMT, potentially by stimulating an autocrine loop of the TGFβ receptor [45]. In our study with cE1 cells dosed with increasing concentration of Ac2-26, we found a two-fold increase in TGF-β1 at the 50 μM dose, which is physiological in consideration to the seminal fluid level of 150 μg/ml. This result was further supported by the evidence that increase in TGF-β1 from treatment with Ac2-26 could be reversed by simultaneous addition of AnxA1 nAb (Fig. 3C). Increase in MAPK and TGFβ activity was supported by qRT-PCR results using cE1 cells grown in Matrigel culture with or without Ac2-26 for 14 days (*Mapk*, $P < 0.05$; *Tgfbr2*, $P < 0.05$; Fig. 3D).

Effect of AnxA1 on cE1 Cells *in vivo*

Next, to substantiate the *in vitro* findings of AnxA1 induction of EMT *in vivo*, the SC^{med} subpopulation of the cE1 cell line was used in renal capsule transplantation technique. Control, CAF CM- or Ac2-26-treated cE1 SC^{med} cells were admixed with UGSM and grafts were transplanted under the renal capsule of non-obese diabetic/severe combined immunodeficient (NOD.SCID) male mice (Supplementary Fig. S4A). The incidence of glandular structure formation was 75% when SC^{med} cells were treated with CAF CM and 100% when treated with Ac2-26; however, no glandular structures were detected in control treated SC^{med} grafts. Staining for androgen receptor (AR) and proliferation marker Ki67 confirmed that the structures seen in CAF CM- and Ac2-26-treated grafts were composed of highly proliferating prostate cancer cells (Fig. 4A, B). Additionally, significant increases in graft size ($P < 0.05$; Supplementary Fig. S4B), number of $p63^+$ cells per graft area ($P < 0.05$) and ratio of $p63^+$ to $CK8^+$ cells per graft area ($P < 0.05$) were observed in Ac2-26 treated SC^{med} cE1 cells (Fig. 4C).

The combined results of SC^{med} transplantation when treated with either CAF CM or Ac2-26 suggested that AnxA1 alone might be able to largely recapitulate the stimulation provided by CAFs in glandular structure formation. These results served as a proof-of-principle that AnxA1 could be a potent secreted factor responsible for the gland-forming stimulation provided by CAFs to CSCs.

Effect of AnxA1 on Primary Tumor LSC$^{hi/med}$ Cells *in vitro*

We proceeded to test the effect of AnxA1 on sorted LSC subpopulations from the *cPten*$^{-/-}$*L* model. As previously described, co-culture of LSC^{hi} cells with CAF led to increasing biological complexity, indicated by formation of multiple basal and luminal layers, as well as immunofluorescent detectable co-expression of basal and luminal cell markers [35]. In the present study, we further observed that spheroids formed after co-culture with CAFs could generate acinar-type projections, a phenotype which was also seen before but not specifically described [35]. Similarly, LSC^{hi} cells grown in the presence of AS-enriched CAF CM fractions, Ac2-26 and rAnxA1 grew complex acinar structures. Expansion of both basal and luminal cell layers after CAF co-culture as well as after treatment with sources of AnxA1 was revealed with IF (Supplementary Fig. S5).

In the previous study, we reported that LSC^{hi} cells co-cultured with CAFs formed greater numbers of spheroids than LSC^{hi} cells co-cultured with UGSM [35]. Here we found that primary cells treated with either mimetic or full-length forms of AnxA1 protein formed more spheroids than the no-treatment control groups. Treatment of LSC^{hi} with Ac2-26 led to a twenty-fold increase over UGSM control, expressed as a percentage of spheroids per total number of cells seeded (control, 0.37% ± 0.006; 5 μM Ac2-26, 14.96% ± 0.35, $P < 0.001$; 50 μM Ac2-26, 23.28% ± 1.7, $P < 0.01$), and murine recombinant full-length AnxA1 (rAnxA1) led to a twenty eight-fold increase (control, 2.47% ± 1.13; 0.5 μM rAnxA1, 9.2% ± 0.85, $P < 0.01$; 5 μM rAnxA1, 13.35% ± 2.15, $P < 0.05$). While LSC^{med} cells virtually lack the ability to form spheroids *in vitro* [35], remarkably greater than 45-fold significant increase in spheroid number was observed in LSC^{med} cells inoculated with rAnxA1 (control, 0.03% ± 0.067; 0.5 μM rAnxA1, 3.6% ± 1.7, *NS*; 5 μM rAnxA1, 28.1% ± 9.27, $P < 0.05$). At least a two-fold difference in spheroid number was observed in LSC^{med} cells treated with Ac2-26 (control, 0.14% ± 0.01; 5 μM Ac2-26, 0.46% ± 0.07, $P < 0.05$; 50 μM Ac2-26, 0.32% ± 0.02, $P < 0.01$; Supplementary Fig. S6A). We observed that LSC$^{hi/med}$ treated with Ac2-26 or rAnxA1 could be passaged for at least up to 3 generations, similar to co-culture with UGSM, demonstrating retention of self-renewal activity in the absence of additional treatment with AnxA1 after the first generation (data not shown).

As shown in Supplementary Fig. S6B, after exposure to increasing concentrations of Ac2-26, LSC^{hi} spheroids evidenced increasing pErk1/2 and TGF-β1 activation. At 50 μM Ac2-26 treatment, greater than 3-fold pErk1/2 activation and 2-fold Erk1/2 activation was seen (pErk1/2, 3.2 ± 0.7, $P <0.01$), compared to control. pErk1/2 activation could be reversed by addition of the AnxA1 nAb in the presence of Ac2-26 (0.5 ± 0.1, $P < 0.01$). Other MAP kinases, p38 and Jnk/Sapk did not show up-regulation of phosphorylation in Ac2-26 treated spheroids relative to control. LSC^{hi} cells showed a 4-fold increase in TGF-β1 at 50 μM Ac2-26 dose (4.2 ± 1.4, $P < 0.001$), compared to control, and significant decrease in response to nAb (0.5 ± 0.4, $P < 0.01$).

Effect of AnxA1 on LSC$^{hi/med}$ Cells *in vivo*

LSC$^{hi/med}$ cells were treated with rAnxA1, Ac2-26 or media control and admixed with UGSM for grafting and transplantation under the renal capsule of NOD.SCID male mice. The histopathology of the grafted cells recovered after 10 week transplantation was

determined. Tumor epithelial cells were shown to be capable of forming glandular structures of three distinct morphological subtypes (Fig. 5 and Fig. 6).

The most frequently observed glandular structure was composed of low cuboidal epithelial cells, characterized by elongated nuclei and low cytoplasmic profile. These structures ranged greatly in size and could comprise sections of the graft up to 300 microns. $p63^+$ cells represented 30–50% of the cells within these structures.

Less frequently, simple cuboidal epithelium was detectably observed as consistent in size and shape and possessed centrally located nuclei that remained uniformly spherical. The size of these glandular structures was reduced, ranging between 50 to 80 microns. Simple cuboidal epithelial structures had the highest percentage of $p63^+$ cells out of all three subtypes, ranging from 70–100% $p63^+$ staining in serial tissue sections.

The third subtype was observed to be composed of high columnar epithelial cells, which were organized into acinar units and which had basolaterally located spherical nuclei and prominent cytoplasm. They displayed higher recruitment of endothelial cells and blood vessels than other glandular subtypes. Columnar, acinar glandular structures were consistently equal to or greater than 300 microns, ranging between 300 to 1500 microns in size. In these structures, $p63^+$ cells comprised 10–20% of the total. Interestingly, their detection was 90% positively correlated with detection of simple cuboidal structures. These histological subtypes were considered noteworthy, although their biological significance would remain to be further explored.

AnxA1 Stimulates Glandular Structure Formation, Differentiation and Proliferation in LSC^{hi} Cells and De-Differentiation in LSC^{med} Cells *in vivo*

Glandular structures were detected in 6/6 (100%) of the rAnxA1 treated LSC^{hi} grafts, 3/5 (60%) of the Ac2-26 treated grafts and 2/5 (40%) of untreated controls (Fig. 5A). LSC^{med} cells were stimulated by AnxA1 to form prostatic glandular structures in 4/4 (100%) of rAnxA1 treated grafts and 4/4 (100%) of Ac2-26 treated grafts. Glandular structures were detected in 0/4 (0%) of untreated controls.

All three morphological glandular subtypes were detected in AnxA1 stimulated LSC^{hi} and LSC^{med} cells (Fig. 5A–B and Fig. 6A–B). LSC^{hi} rAnxA1 treated grafts were most stimulated to form both cuboidal and acinar type glandular structures, which were found to co-occur in 4/6 (67%) of the grafts (Fig. 5A, B). In LSC^{med} grafts, acinar type glandular structures were present in 2/4 (50%) of rAnxA1 treated grafts, 1/4 (25%) of Ac2-26 treated grafts and 0/4 (0%) of control grafts. Simple cuboidal glandular structures were only detected in rAnxA1 treated grafts (Fig. 6A, B).

All glandular structures detected were stained for CRE and PTEN to confirm the presence of $Cre^+/Pten^-$ cells of $cPten^{-/-}L$ origin (representative CRE and PTEN staining depicted in Supplementary Fig. S7). Histological analyses of all three treatment groups in LSC^{hi} and LSC^{med} grafts revealed $AR^+/CRE^+/PTEN^-$ prostate epithelial cells. Ac2-26 and rAnxA1 stimulated $LSC^{hi/med}$ cells formed glandular structures with higher abundance of basal marker $p63^+$, luminal marker $CK8^+$ and $Ki67^+$ cells than untreated controls (LSC^{hi} Ki67:

control, 6.83% ± 3.62; Ac2-26, 15.64% ± 2.74, $P < 0.01$; rAnxA1, 14.79% ± 4.84, $P < 0.05$. LSC^{med} Ki67: control, 8.74% ± 11.85; Ac2-26, 7.37% ± 5.99, *NS*; rAnxA1, 12.27% ± 2.56, *NS*). In contrast $LSC^{hi/med}$ untreated control grafts were mostly comprised of $CK8^{+}$, $Ki67^{-}$ cells, indicating less-proliferative, differentiated cells. LSC^{med} untreated control grafts had virtually no detectable $p63^{+}$ staining. Treatment with Ac2-26 and rAnxA1 led to significantly greater expression of p63 (LSC^{hi}: Ac2-26, $P < 0.01$; rAnxA1, $P < 0.001$. LSC^{med}: Ac2-26, $P < 0.001$; rAnxA1, $P < 0.01$) and ratio of $p63^{+}$ to $CK8^{+}$ cells per graft area (LSC^{hi}: Ac2-26, $P < 0.05$; rAnxA1, $P < 0.05$. LSC^{med}: Ac2-26, *NS*; rAnxA1, $P < 0.05$; Fig. 5C–D and Fig. 6C–D). Among all $LSC^{hi/med}$ grafts, highest p63 expression was observed in simple cuboidal glandular structures compared to the other two subtypes (acinar, 17.6% ± 5.8; low cuboidal, 40.9% ± 8.5, $P < 0.01$; simple cuboidal, 83.4% ± 10, $P < 0.001$).

In AnxA1 treated grafts where glandular structures were detected, larger areas of the graft were found to be covered by glandular formation compared to untreated controls. LSC^{hi} Ac2-26 and rAnxA1 stimulated cells formed larger structures than controls, multiple structures per graft were present, and more $CK8^{+}$ cells were observed, particularly in acinar glandular structures. AnxA1 treatment stimulated LSC^{med} cells to form glandular structures compared to controls, and in acinar structures, more $CK8^{+}$ cells were observed. Observations in acinar type structures accounted for the significant differences in size and number of glandular structures detected in AnxA1 treated groups, especially LSC^{med} (Fig. 6E and Supplementary Fig. S8).

We next analyzed the status of Erk1/2 and pErk1/2. Glandular structures possessed Erk1/2 and pErk1/2 positive foci, indicating a possible stable up-regulation of the pErk1/2 pathway due to stimulation by AnxA1, as similarly seen *in vitro*. pErk1/2 expression was two- to three-fold higher in Ac2-26 and rAnxA1 treated $LSC^{hi/med}$ than control $LSC^{hi/med}$ grafts, after normalization to Erk expression and proliferation marker Ki67 (Normalized fold changes compared to controls. LSC^{hi} pErk1/2: Ac2-26, 1.4 ± 0.4, $P < 0.05$; rAnxA1, 1.6 ± 0.3, $P < 0.05$. LSC^{med} pErk1/2: Ac2-26, 3.0 ± 0.3, $P < 0.01$; rAnxA1, 2.2 ± 0.3, $P < 0.01$; Supplementary Fig. S9A–D).

Effect of AnxA1 on LNCaP and PC3 Cells *in vitro*

We tested the effect of AnxA1 on cells from human-derived prostate cancer. LNCaP and PC3 cell lines were treated with vehicle control, 5 μM or 50 μM Ac2-26, and were assayed for spheroid formation at 3 and 6 days. Both LNCaP and PC3 cells formed greater numbers of spheroids after treatment with Ac2-26 at both concentrations, at days 3 and 6, compared to controls (Fig. 7A). Moreover, larger spheroids were counted in treated versus untreated wells at 6 days (Fig. 7B).

Discussion

We sought to identify secreted factors from the CAFs that are capable of contributing to the generation of CSCs. We demonstrate that AnxA1 is secreted by the CAF cells of the prostate tumor mouse model. The CSC subpopulation can be induced to increased differentiation potential and proliferation following exposure to extracellular AnxA1. This recapitulates many of the observations made when CSCs were tested before in co-cultures

with CAFs [35]. Thus, it appears that AnxA1 is a potent and prominent factor among the various secretory molecules that are produced by the CAFs in the tumor microenvironment, particularly in relation to the stimulation of CSC activity.

Our data furthermore supports that AnxA1 is capable of promoting *de novo* generation of CSCs from prostate cancer cells in addition to stimulating the CSC population. Presumably, EMT-like transition seen *in vitro* may be linked to a process of CSC generation. For example, AnxA1-induced EMT in SC^{med} cells appears to correlate with its capability to enhance formation of prostatic glandular structures when these cells are transplanted *in vivo*. Similarly, the more differentiated primary subpopulation, LSC^{med}, when treated with AnxA1 displays a gain of CSC properties not possessed intrinsically. Significant gain of ability to form spheroids *in vitro* and glandular structures *in vivo* is seen. Moreover, LSC^{med} cells stimulated by AnxA1 show plasticity in regards to size, number and morphological types of glandular structures formed that is akin to that of the LSC^{hi} cells. Because LSC^{med} cells do not display capability to exhibit these behaviors in the absence of treatment, their response to AnxA1 is even more relevant to the premise that AnxA1 appears to shift the cancer cells back to a more stem cell-like state. LSC^{hi}, known to harbor CSCs, also respond to AnxA1 treatment by exhibiting enhanced CSC-like activity *in vitro* and *in vivo*, compared to untreated controls. In this regard, like the mouse prostate cancer cells, spheroid-forming capability of subpopulations present in human prostate cancer cell lines, LNCaP and PC-3 was also found to be enhanced by AnxA1.

In this study, LSC^{med} were stimulated by AnxA1 *in vitro*. This is in slight contrast to the previous study in which LSC^{med} co-cultured with CAFs were not stimulated for increased spheroid formation [35]. However, there we conducted co-culture of stromal cells to epithelial cells at a ratio to 1:1. For the *in vitro* studies here, we used a ratio of 10:1, a composition reported in the literature to be optimal for recapitulating biological effects [46]. LSC^{med} cells appear to be more sensitive to dose-dependent effects, as spheroid formation was significantly stimulated over controls at the higher concentration of rAnxA1. Similar, but distinctly less pronounced, spheroid formation was noted using the mimetic peptide, again stressing the relative sensitivity of this fraction of tumor cells to concentration and potency of stimulant, compared to LSC^{hi}.

AnxA1 treatment significantly increases the incidence of simple cuboidal structures with highest p63 expression and acinar glandular structures, which are greatest in size. Moreover, these structures are more commonly seen in rAnxA1 treated than Ac2-26 treated grafts. Cuboidal and acinar structures are not seen in untreated LSC^{med} controls and are greatly reduced in LSC^{hi} controls. These findings may suggest that exposure to AnxA1 increases the inherent plasticity of tumor epithelial cells to form more complex structures and different morphologies. This additionally supports the supposition that cells exposed to AnxA1 may have undergone an EMT, contributing to their plasticity.

A possible reason for the observed differences in effects seen with the full-length protein versus the mimetic Ac2-26 peptide may be the support of the N-terminal domain of the full-length by the pore from the 4 α-helical repeats, which create a “doughnut-like” ring around that domain. The pore may, thus, stabilize physical interaction of the N-terminus of the full-

length protein with the bound receptor and with an adjacent receptor or protein [47–49]. Possibly stabilized interaction of the full-length may selectively lead to greater activation of signaling downstream of Fpr-rs1, whereas the lower stability and promiscuity of mimetic Ac2-26 may lead to activation of Fpr1, Fpr-rs1 and Fpr-rs2 and other downstream pathways, albeit with less potent constitutive activity [6, 12, 21, 25, 27].

Our overall results suggest that AnxA1 from CAFs may contribute to tumor stem cell activity via two separate but complementary pathways: (1) induction of a de-differentiation process, an intermediate step being akin to EMT, leading to generation of basal stem-like cells, and (2) enhancement of the proliferation and differentiation of the cancer stem cells. AnxA1 is thus implicated in a paradigm in which cells that are malignant epithelial but not cancer stem cells can be induced to gain cancer stem cell-like properties, and cells that already possess the properties of cancer stem cells can be enhanced for their oncologic properties. We find that AnxA1 treatment can significantly increase pErk1/2 activation and TGF-β1/TGFβRII in cE1 and LSC cells. These observations remain to be further developed for a mechanistic scrutiny of AnxA1 effect.

Additionally, as indicated by regression analysis of AnxA1 relative to tumor size, CAF cells may potentially produce higher levels of phospho-Ser^{27}-AnxA1 as disease progresses. Thus, as a possible logical extension of our findings to the study of human prostate, an analysis of stromal AnxA1 expression in normal prostates, stratified by advancing age, and in prostate tumors at different stages of disease progression may be worthwhile. It is noteworthy that AnxA1 is naturally most abundant in the seminal fluid [11] and seminal vesicles are most closely associated with the prostate gland. In this regard, it is possible to speculate that phospho-Ser^{27}-AnxA1 produced in tumors may be detectable in seminal fluid.

Finally, a role for AnxA1 may be viewed in the context of therapy. Cancer cells (or their progenitors) are constantly evolving, thereby developing resistance to therapy. In contrast, fibroblast cells of the tumor microenvironment are less evolving and thus may provide a more stable target for. AnxA1 is an important factor coming from the prostate stroma, and is now shown, at least in a model system, to support the prostate cancer stem cell niche through maintenance and *de novo* generation of basal stem-like cancer cells *in vivo*. Therefore, potential therapies interrupting the CAF-AnxA1-CSC axis may prove to be a rational adjuvant approach for the treatment of prostate cancers.

Supplementary Material

Refer to Web version on PubMed Central for supplementary material.

Acknowledgments

We would like to thank Lora Barsky and David Stanley at the USC Flow Cytometry Core for technical assistance, as well as the Imaging Core for use of their microscopes for capture of IF images. We additionally acknowledge members of the Zandi laboratory for assistance in providing materials and training for silver staining and the Proteomics Core for mass spectrometry.

Grant support

This work was supported by the NIH grant RO1CA059705 to P. Roy-Burman. Additionally, the project was partially supported by a supplemental diversity award from the NCI to L. Geary, number 3 RO1CA059705-17S1. The content is solely the responsibility of the authors and does not necessarily represent the official views of the National Cancer Institute or the National Institutes of Health.

Abbreviations

CSC	cancer stem cell
CRPC	castration-resistant prostate cancer
AnxA1	annexin a1
CAF	cancer-associated fibroblasts
NPF	normal prostate fibroblasts
UGSM	urogenital sinus mesenchyme
CM	conditioned medium
EMT	epithelial-to-mesenchymal transition
AS	ammonium sulfate
L (Lin)	lineage
S (SCA-1)	stem cell antigen-1
C (CD49f)	α-6 integrin
PKC	protein kinase C
FPR	formyl peptide receptor

References

1. Crompton MR, Moss SE, Crumpton MJ. Diversity in the lipocortin/calpactin family. Cell. 1988; 55(1):1–3. [PubMed: 2971450]
2. Crumpton MJ, Dedman JR. Protein terminology tangle. Nature. 1990; 345(6272):212. [PubMed: 2333094]
3. Raynal P, Pollard HB. Annexins: the problem of assessing the biological role for a gene family of multifunctional calcium- and phospholipid-binding proteins. Biochim Biophys Acta. 1994; 1197(1): 63–93. [PubMed: 8155692]
4. Blackwell GJ, Carnuccio R, Di Rosa M, Flower RJ, Parente L, Persico P. Macrocortin: a polypeptide causing the anti-phospholipase effect of glucocorticoids. Nature. 1980; 287(5778):147–149. [PubMed: 6893620]
5. Miele L, Cordella-Miele E, Facchiano A, Mukherjee AB. Novel anti-inflammatory peptides from the region of highest similarity between uteroglobin and lipocortin I. Nature. 1988; 335(6192):726–730. [PubMed: 2971881]
6. Gavins FN, Yona S, Kamal AM, Flower RJ, Perretti M. Leukocyte antiadhesive actions of annexin 1: ALXR- and FPR-related anti-inflammatory mechanisms. Blood. 2003; 101(10):4140–4147. [PubMed: 12560218]
7. Getting SJ, Flower RJ, Perretti M. Inhibition of neutrophil and monocyte recruitment by endogenous and exogenous lipocortin 1. Br J Pharmacol. 1997; 120(6):1075–1082. [PubMed: 9134220]
8. Parente L, Solito E. Annexin 1: more than an anti-phospholipase protein. Inflamm Res. 2004; 53(4): 125–132. [PubMed: 15060718]

9. Hsiang CH, Tunoda T, Whang YE, Tyson DR, Ornstein DK. The impact of altered annexin I protein levels on apoptosis and signal transduction pathways in prostate cancer cells. Prostate. 2006; 66(13):1413–1424. [PubMed: 16741918]
10. Skouteris GG, Schroder CH. The hepatocyte growth factor receptor kinase-mediated phosphorylation of lipocortin-1 transduces the proliferating signal of the hepatocyte growth factor. J Biol Chem. 1996; 271(44):27266–27273. [PubMed: 8910300]
11. Christmas P, Callaway J, Fallon J, Jones J, Haigler HT. Selective secretion of annexin 1, a protein without a signal sequence, by the human prostate gland. J Biol Chem. 1991; 266(4):2499–2507. [PubMed: 1824943]
12. D'Acquisto F, Perretti M, Flower RJ. Annexin-A1: a pivotal regulator of the innate and adaptive immune systems. Br J Pharmacol. 2008; 155(2):152–169. [PubMed: 18641677]
13. Perretti M, Croxtall JD, Wheller SK, Goulding NJ, Hannon R, Flower RJ. Mobilizing lipocortin 1 in adherent human leukocytes downregulates their transmigration. Nat Med. 1996; 2(11):1259–1262. [PubMed: 8898757]
14. Chapman LP, Epton MJ, Buckingham JC, Morris JF, Christian HC. Evidence for a role of the adenosine 5'-triphosphate-binding cassette transporter A1 in the externalization of annexin I from pituitary folliculo-stellate cells. Endocrinology. 2003; 144(3):1062–1073. [PubMed: 12586783]
15. Morris JF, Christian HC, Chapman LP, Epton MJ, Buckingham JC, Ozawa H. Steroid effects on secretion from subsets of lactotrophs: role of folliculo-stellate cells and annexin 1. Arch Physiol Biochem. 2002; 110(1–2):54–61. [PubMed: 11935401]
16. Payne CM, Morris JF, Solito E, Buckingham JC. Modulators of the SUR2B/Kir6.1 ATP-sensitive K+channel regulate annexin 1 release in the TtT/GF folliculostellate cell line. 24th Joint Meeting of the British Endocrine Societies. 2005
17. Wein S, Fauroux M, Laffitte J, de Nadai P, Guaini C, Pons F. Mediation of annexin 1 secretion by a probenecid-sensitive ABC-transporter in rat inflamed mucosa. Biochem Pharmacol. 2004; 67(6): 1195–1202. [PubMed: 15006554]
18. John CD, Christian HC, Morris JF, Flower RJ, Solito E, Buckingham JC. Kinase-dependent regulation of the secretion of thyrotrophin and luteinizing hormone by glucocorticoids and annexin 1 peptides. J Neuroendocrinol. 2003; 15(10):946–957. [PubMed: 12969239]
19. Solito E, Christian HC, Festa M, Mulla A, Tierney T, Flower RJ. Post-translational modification plays an essential role in the translocation of annexin A1 from the cytoplasm to the cell surface. FASEB J. 2006; 20(9):1498–1500. [PubMed: 16720734]
20. Solito E, Mulla A, Morris JF, Christian HC, Flower RJ, Buckingham JC. Dexamethasone induces rapid serine-phosphorylation and membrane translocation of annexin 1 in a human folliculostellate cell line via a novel nongenomic mechanism involving the glucocorticoid receptor, protein kinase C, phosphatidylinositol 3-kinase, and mitogen-activated protein kinase. Endocrinology. 2003; 144(4):1164–1174. [PubMed: 12639897]
21. John CD, Gavins FN, Buss NA, Cover PO, Buckingham JC. Annexin A1 and the formyl peptide receptor family: neuroendocrine and metabolic aspects. Curr Opin Pharmacol. 2008; 8(6):765–776. [PubMed: 18845272]
22. Lange C, Starrett DJ, Goetsch J, Gerke V, Rescher U. Transcriptional profiling of human monocytes reveals complex changes in the expression pattern of inflammation-related genes in response to the annexin A1-derived peptide Ac1-25. J Leukoc Biol. 2007; 82(6):1592–1604. [PubMed: 17855500]
23. Perretti M, D'Acquisto F. Annexin A1 and glucocorticoids as effectors of the resolution of inflammation. Nat Rev Immunol. 2009; 9(1):62–70. [PubMed: 19104500]
24. Tagoe CE, Marjanovic N, Park JY, Chan ES, Abeles AM, Attur M. Annexin-1 mediates TNF-alpha-stimulated matrix metalloproteinase secretion from rheumatoid arthritis synovial fibroblasts. J Immunol. 2008; 181(4):2813–2820. [PubMed: 18684973]
25. Ernst S, Lange C, Wilbers A, Goebeler V, Gerke V, Rescher U. An annexin 1 N-terminal peptide activates leukocytes by triggering different members of the formyl peptide receptor family. J Immunol. 2004; 172(12):7669–7676. [PubMed: 15187149]

26. Perretti M, Chiang N, La M, Fierro IM, Marullo S, Getting SJ. Endogenous lipid- and peptide-derived anti-inflammatory pathways generated with glucocorticoid and aspirin treatment activate the lipoxin A4 receptor. Nat Med. 2002; 8(11):1296–1302. [PubMed: 12368905]
27. Hayhoe RP, Kamal AM, Solito E, Flower RJ, Cooper D, Perretti M. Annexin 1 and its bioactive peptide inhibit neutrophil-endothelium interactions under flow: indication of distinct receptor involvement. Blood. 2006; 107(5):2123–2130. [PubMed: 16278303]
28. Lim LH, Pervaiz S. Annexin 1: the new face of an old molecule. FASEB J. 2007; 21(4):968–975. [PubMed: 17215481]
29. Kang JS, Calvo BF, Maygarden SJ, Caskey LS, Mohler JL, Ornstein DK. Dysregulation of annexin I protein expression in high-grade prostatic intraepithelial neoplasia and prostate cancer. Clin Cancer Res. 2002; 8(1):117–123. [PubMed: 11801547]
30. Patton KT, Chen HM, Joseph L, Yang XJ. Decreased annexin I expression in prostatic adenocarcinoma and in high-grade prostatic intraepithelial neoplasia. Histopathology. 2005; 47(6): 597–601. [PubMed: 16324197]
31. Paweletz CP, Ornstein DK, Roth MJ, Bichsel VE, Gillespie JW, Calvert VS. Loss of annexin 1 correlates with early onset of tumorigenesis in esophageal and prostate carcinoma. Cancer Res. 2000; 60(22):6293–6297. [PubMed: 11103786]
32. Smitherman AB, Mohler JL, Maygarden SJ, Ornstein DK. Expression of annexin I, II and VII proteins in androgen stimulated and recurrent prostate cancer. J Urol. 2004; 171(2 Pt 1):916–920. [PubMed: 14713853]
33. Xin W, Rhodes DR, Ingold C, Chinnaiyan AM, Rubin MA. Dysregulation of the annexin family protein family is associated with prostate cancer progression. Am J Pathol. 2003; 162(1):255–261. [PubMed: 12507908]
34. Khau T, Langenbach SY, Schuliga M, Harris T, Johnstone CN, Anderson RL. Annexin-1 signals mitogen-stimulated breast tumor cell proliferation by activation of the formyl peptide receptors (FPRs) 1 and 2. FASEB J. 2011; 25(2):483–496. [PubMed: 20930115]
35. Liao CP, Adisetiyo H, Liang M, Roy-Burman P. Cancer-associated fibroblasts enhance the gland-forming capability of prostate cancer stem cells. Cancer Res. 2010; 70(18):7294–7303. [PubMed: 20807814]
36. Liao CP, Liang M, Cohen MB, Flesken-Nikitin A, Jeong JH, Nikitin AY. Mouse models of prostate adenocarcinoma with the capacity to monitor spontaneous carcinogenesis by bioluminescence or fluorescence. Cancer Res. 2007; 67(15):7525–7533. [PubMed: 17671224]
37. Wang S, Gao J, Lei Q, Rozengurt N, Pritchard C, Jiao J. Prostate-specific deletion of the murine Pten tumor suppressor gene leads to metastatic prostate cancer. Cancer Cell. 2003; 4(3):209–221. [PubMed: 14522255]
38. Xin L, Lukacs RU, Lawson DA, Cheng D, Witte ON. Self-renewal and multilineage differentiation in vitro from murine prostate stem cells. Stem Cells. 2007; 25(11):2760–2769. [PubMed: 17641240]
39. Yang S, Pham LK, Liao CP, Frenkel B, Reddi AH, Roy-Burman P. A novel bone morphogenetic protein signaling in heterotypic cell interactions in prostate cancer. Cancer Res. 2008; 68(1):198–205. [PubMed: 18172312]
40. Liao CP, Liang M, Cohen MB, Flesken-Nikitin A, Jeong JH, Nikitin AY. Mouse prostate cancer cell lines established from primary and postcastration recurrent tumors. Horm Cancer. 2010; 1(1): 44–54. [PubMed: 20631921]
41. Burgess RR. Protein precipitation techniques. Methods Enzymol. 2009; 463:331–342. [PubMed: 19892180]
42. Lukacs RU, Goldstein AS, Lawson DA, Cheng D, Witte ON. Isolation, cultivation and characterization of adult murine prostate stem cells. Nat Protoc. 2010; 5(4):702–713. [PubMed: 20360765]
43. Lawson DA, Xin L, Lukacs RU, Cheng D, Witte ON. Isolation and functional characterization of murine prostate stem cells. Proc Natl Acad Sci U S A. 2007; 104(1):181–186. [PubMed: 17185413]

44. Mulholland DJ, Xin L, Morim A, Lawson D, Witte O, Wu H. Lin-Sca-1+CD49fhigh stem/progenitors are tumor-initiating cells in the Pten-null prostate cancer model. Cancer Res. 2009; 69(22):8555–8562. [PubMed: 19887604]
45. de Graauw M, van Miltenburg MH, Schmidt MK, Pont C, Lalai R, Kartopawiro J. Annexin A1 regulates TGF-beta signaling and promotes metastasis formation of basal-like breast cancer cells. Proc Natl Acad Sci U S A. 2010; 107(14):6340–6345. [PubMed: 20308542]
46. Lawson DA, Xin L, Lukacs R, Xu Q, Cheng D, Witte ON. Prostate stem cells and prostate cancer. Cold Spring Harb Symp Quant Biol. 2005; 70:187–196. [PubMed: 16869753]
47. Bitto E, Li M, Tikhonov AM, Schlossman ML, Cho W. Mechanism of annexin I-mediated membrane aggregation. Biochemistry. 2000; 39(44):13469–13477. [PubMed: 11063583]
48. Lambert O, Gerke V, Bader MF, Porte F, Brisson A. Structural analysis of junctions formed between lipid membranes and several annexins by cryo-electron microscopy. J Mol Biol. 1997; 272(1):42–55. [PubMed: 9299336]
49. Mailliard WS, Haigler HT, Schlaepfer DD. Calcium-dependent binding of S100C to the N-terminal domain of annexin I. J Biol Chem. 1996; 271(2):719–725. [PubMed: 8557678]

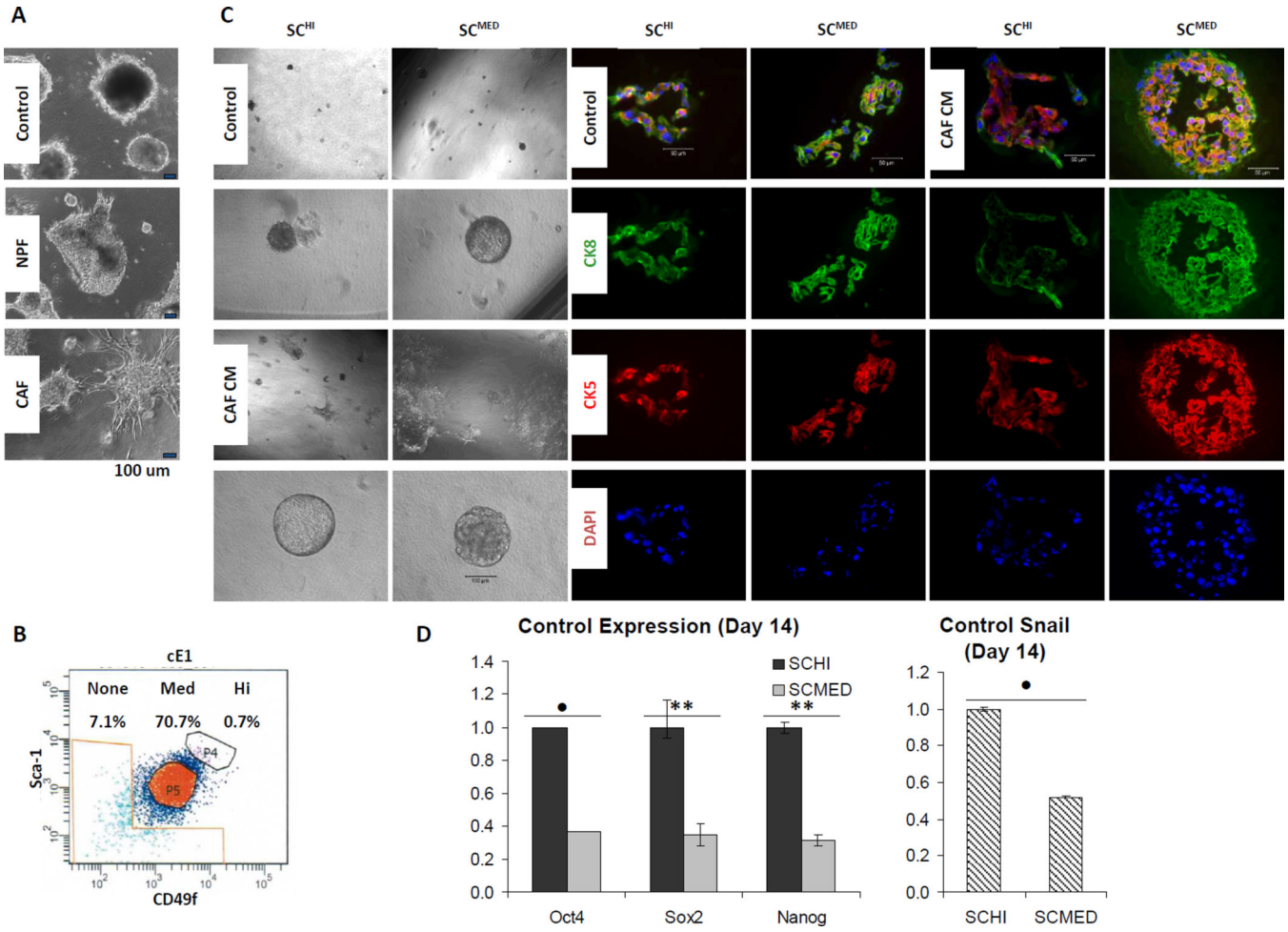

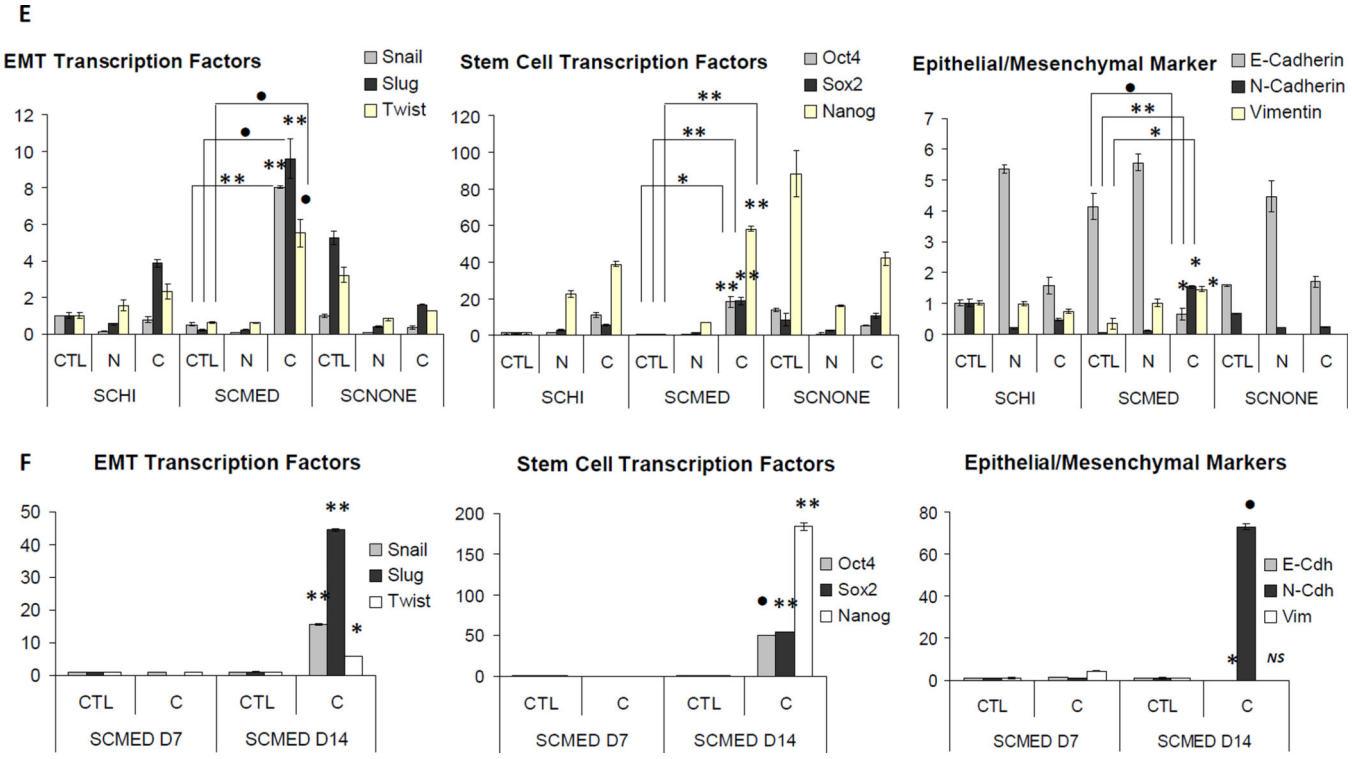

Figure 1.

CAFs induce EMT to cE1 mouse prostate cancer cells *in vitro*. A, phase contrast images of representative spheroids formed in cE1, after co-culturing with either control media, NPFs or CAFs. Bar 100 μm. B, cE1 cells were FACS sorted into subpopulations based on high, medium and no expression of SCA-1 (S) and CD49f (C; SC^{hi}, SC^{med} and SC^{none}, respectively). C, Sorted cells grown in post-FACS 3-D culture displayed differential response to CAF CM. cE1 SC^{hi} and SC^{med} spheroids increased in size in the presence of CAF CM. Phase contrast images show gross spheroid morphology and incidence of EMT-like phenotypic changes in CAF CM treated cE1 SC^{med} cells. Sections of spheroids were analyzed by coimmunofluorescence (co-IF) using antibodies against the basal/transit-amplifying cell marker CK5 (red) and luminal cell marker CK8 (green). 4',6-Diamidino-2-phenylindole (DAPI) was used to label cell nuclei. Phase contrast, bar 100 μm; IF, bar 50 μm. D, Grown in maintenance media, SC^{hi} and SC^{med} displayed distinguishing molecular characteristics as assessed by expression levels of pluripotency transcription factors Oct4, Nanog and Sox2, and Snail. E, Expression of EMT/pluripotency transcription factors increases after 14 days in SC^{med} via CAF CM treatment. SC^{hi}, SC^{med} and SC^{none} cells were subjected to control media (CTL), NPF CM (N) or CAF CM (C) for 14 days. SC^{med} + CAF CM was compared to SC^{hi} + CAF CM and SC^{none} + CAF CM (indicated above bars) as described in the text, SC^{med} + control (indicated above lines), and SC^{med} + NPF CM (data not shown). Induction of EMT in response to CAF CM in cE1 SC^{med} cells was confirmed by qRT-PCR using EMT transcription factor markers Snail, Slug and Twist, pluripotency transcription factors Oct4, Sox2 and Nanog, epithelial marker E-cadherin, and mesenchymal markers N-cadherin and Vimentin. F, Up-regulation of EMT and pluripotency transcription factors, as well as mesenchymal markers, and decrease in E-cadherin in SC^{med} cells exposed

to CAF CM was observed between 7 and 14 days of treatment, compared to control. All qRT-PCR ratios are expressed as fold change normalized to β-Actin expression. In all panels, CAFs 1 and 3 were used in independent repeats. *NS*, not significant; *, $P < 0.05$; •, $P < 0.01$; **, $P < 0.001$.

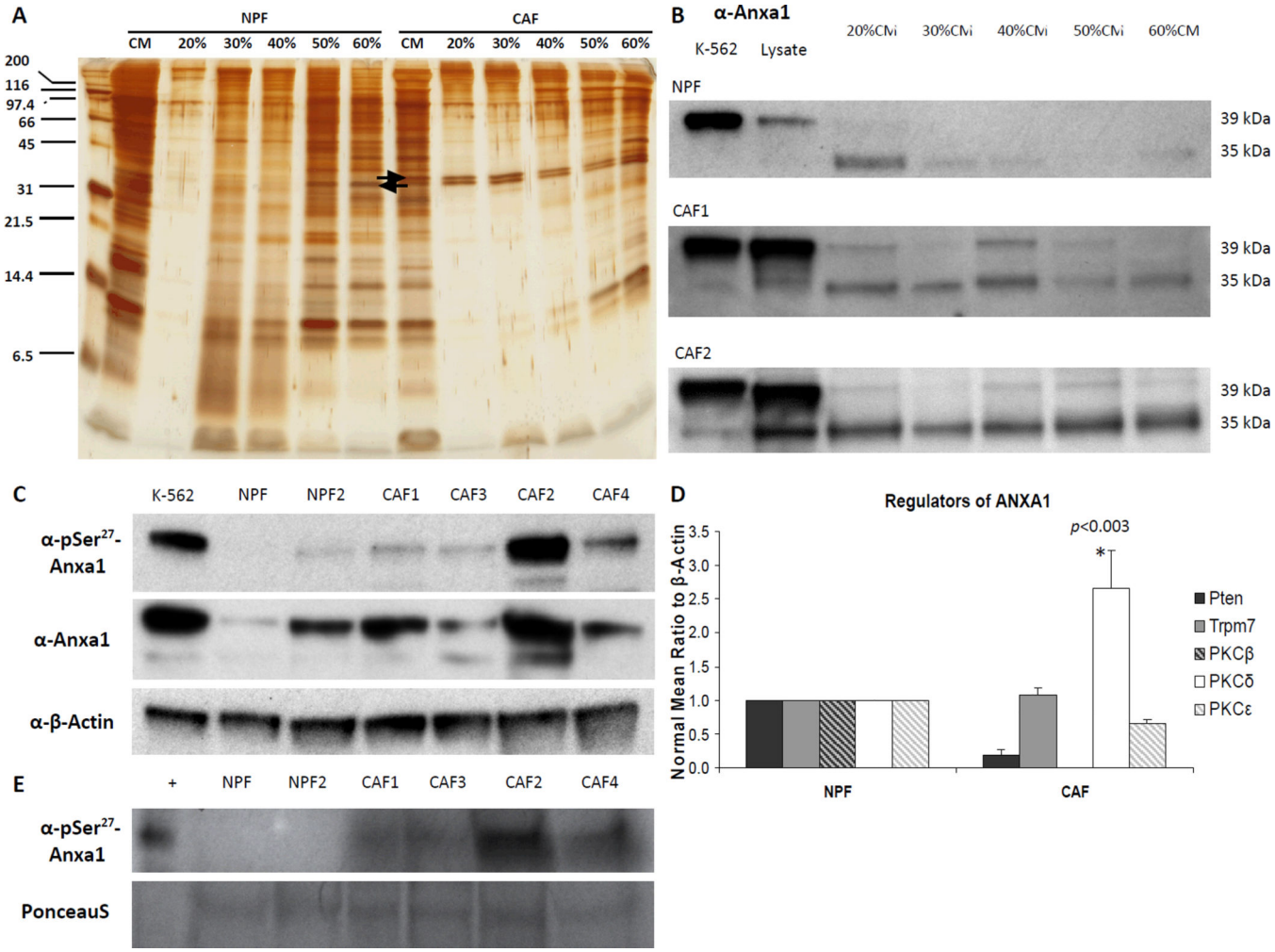

Figure 2.

AnxA1 is secreted from CAF. A, AS precipitated NPF and CAF CM protein fractions were run on an electrophoresis gel for silver stain. A pronounced band was found to be present in the CAF CM and CAF CM AS fractions. This band was weak or lacking in the NPF CM or NPF CM AS fractions. CAF CM AS bands were removed and analyzed using mass spectrometry (MS). AnxA1 was implicated from the results of MS. B, Western blot using antibody against AnxA1 confirmed the presence of AnxA1 in stromal cultures. K-562 positive control lysate was used as a loading control for exposure time between western blots of CM fractions. α-AnxA1 stained positive for two bands in blots in NPF CM fractions, CAF and CAF CM fractions. Both bands were more robust in CAF and CAF CM fractions compared to NPF, and the upper band that was more prevalent in CAF CM fractions was correlated with biological activity (Supplementary Fig. S2). Highest abundance of AnxA1 was found in the 30–40% AS cut of CAF CM. C, Phospho-serine specific antibody recognizing the amino acid motif ± 3 amino acids surrounding p-Ser^{27} against NPF and CAF lysates revealed more p-Ser^{27}–AnxA1 in CAF upper band. D, Serine phosphorylator, PKCδ is upregulated in CAF. K-562 is positive control for AnxA1. *, P < 0.01. E, Phospho-serine specific antibody recognizing the amino acid motif ± 3 amino acids

surrounding p-Ser^{27} against NPF and CAF CM revealed more p-Ser^{27}–AnxA1 present in CM from CAFs than NPFs. CAF2 lysate was used as a positive control. Equal loading was assessed by Ponceau S solution stain.

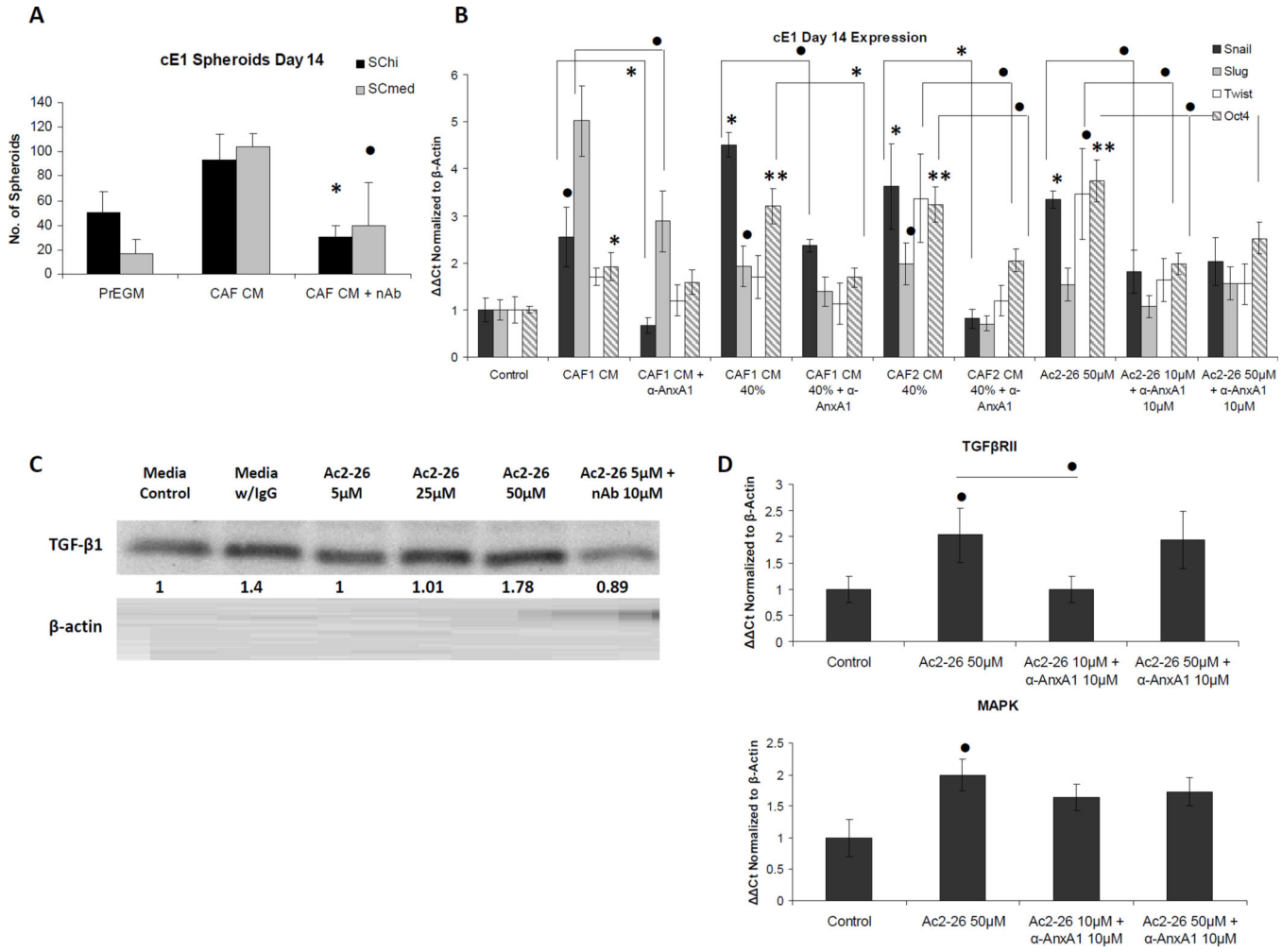

Figure 3.

Effect of α-AnxA1 neutralizing antibody (nAb) on spheroids and EMT of cE1 cells. A, Addition of α-AnxA1 nAb to cE1 SC^{hi} and SC^{med} cells reduced the number of spheroids grown in the presence of CAF CM. B, Unsorted cE1 cells showed increase in expression of Snail, Slug, Twist, and Oct4 after treatment with CAF CM, AnxA1 enriched CAF CM AS fraction from two CAF cultures (CAF1 and CAF2 in parallel western blot analyses) and Ac2-26. cE1 cells treated with α-AnxA1 nAb in the presence of CAF CM, AnxA1 enriched CAF CM AS fractions and Ac2-26 had reduced expression of Snail, Slug, Twist and Oct4. All conditions were analyzed using untreated media control and compared to the experimental control condition of media + IgG. CAF1 and CAF2 were used for two independent repeats, and CAF3 was analyzed in two additional independent repeats. C–D, Analysis of pathways associated with AnxA1. C, α-TGFβ western blots revealed close to two-fold increase in TGF-β1 after treatment of cE1 spheroids with increasing concentrations of Ac2-26, compared to expression in media control and media + IgG. TGF-β1 expression was reduced after α-AnxA1 nAb was combined with Ac2-26 treatment. D, qRT-PCR indicated activation of MAPK and TGFβ pathways, as shown by significant increase in *Mapk* and *Tgfbr2* expression after addition of Ac2-26 to cE1 cells grown in 3-D culture.

Control is media with IgG. In all panels, statistical significance is indicated by •, $P < 0.05$; *, $P < 0.01$; **, $P < 0.001$.

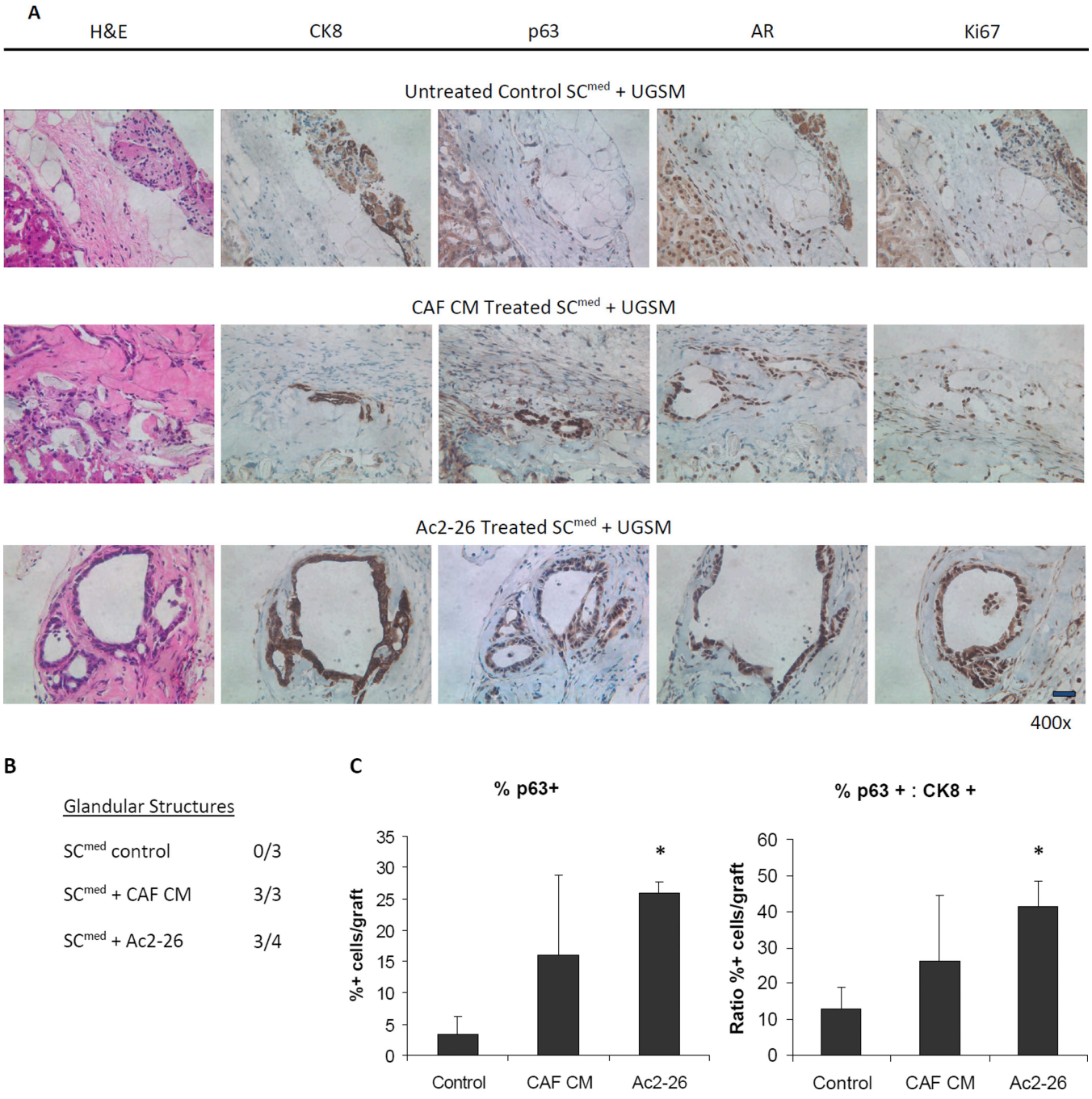

Figure 4.

Characteristics of SC^{med} cells treated with CAF CM and Ac2-26 and grown under the renal capsule of NOD.SCID male mice *in vivo*. A, Hematoxylin and eosin (H&E) and immunohistochemistry (IHC) images of representative untreated, CAF CM treated and Ac2-26 treated cE1 SC^{med} cells reveal the formation of glandular structures in CAF CM treated and Ac2-26 treated grafts. Treated grafts possessed increased basal and proliferating prostate cancer cells as analyzed by IHC for p63, CK8, AR, and Ki67. Images at 400× magnification. Bar 100 μm. B, Incidence of grafts with detectable glandular structures. C,

Basal cell expansion was quantified from the number of $p63^+$ cells per total cells per graft area and the ratio of $p63^+$ cells to $CK8^+$ cells per total cells per graft area. *, $P < 0.05$.

A

Glandular Structures	
LSC^{hi} control	2/5
LSC^{hi} + Ac2-26	3/5
LSC^{hi} + rAnxa1	6/6
Acinar Glandular Structures	
LSC^{hi} control	1/5
LSC^{hi} + Ac2-26	0/5
LSC^{hi} + rAnxa1	4/6

B

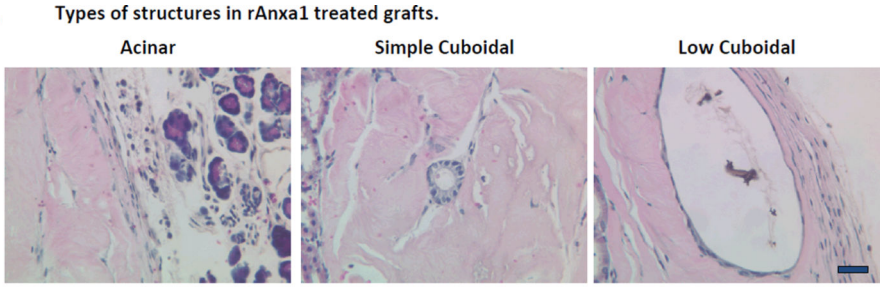

C

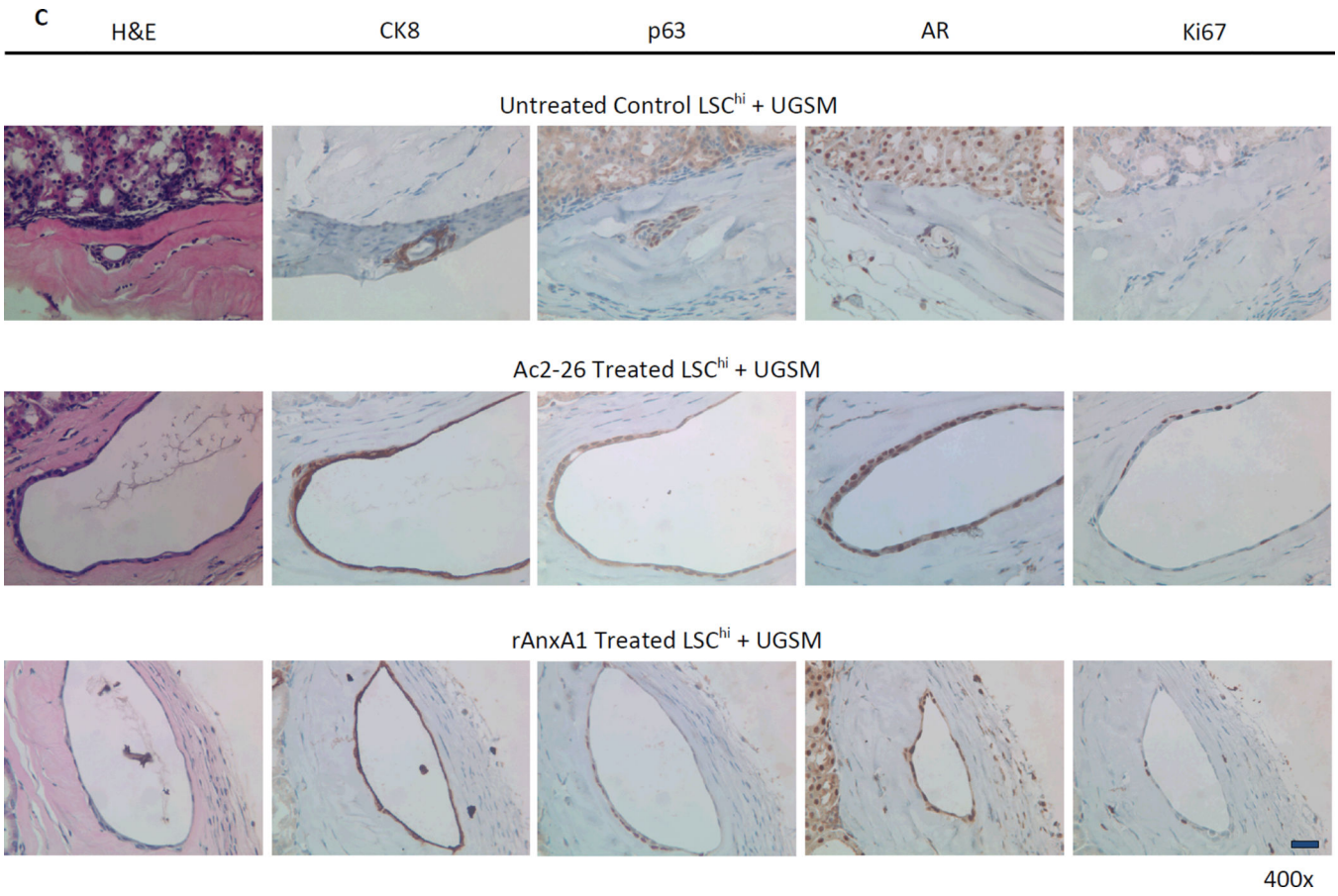

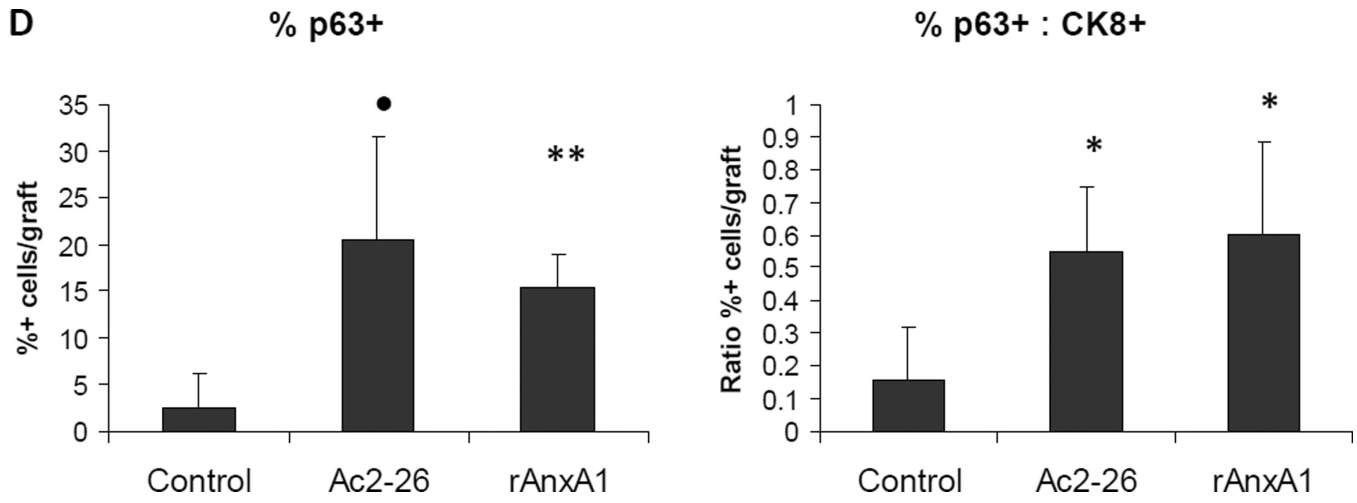

Figure 5.

Effect of AnxA1 on incidence, types, differentiation and proliferation of glandular structures in LSC^{hi} grafts. A, Chart depicting the incidence and type of glandular structures (cuboidal or acinar type glandular) scored in LSC^{hi} untreated control, Ac2-26 treated and rAnxA1 treated grafts. B, Representative H&E images of the types of structures detected in rAnxA1 treated grafts. Magnification at 400×. Bar 100 μm. C, Tissue sections were analyzed by H&E for basic histology and IHC for expression of basal cell marker p63, luminal cell marker CK8, androgen receptor (AR) and Ki67. Magnification at 400×. Bar 100 μm. D, Calculated percentage of $p63^+$ cells and ratio of $p63^+$ to $CK8^+$ cells detected in the grafts. Potential to undergo de-differentiation in response to AnxA1 was assessed by increase in p63 expression compared to CK8. Statistical significance is indicated by *, $P < 0.05$; •, $P < 0.01$; **, $P < 0.001$.

A

Glandular Structures	
LSC^{med} control	0/4
LSC^{med} + Ac2-26	4/4
LSC^{med} + rAnxa1	4/4
Acinar Glandular Structures	
LSC^{med} control	0/4
LSC^{med} + Ac2-26	1/4
LSC^{med} + rAnxa1	2/4

B Types of structures in rAnxa1 treated grafts.

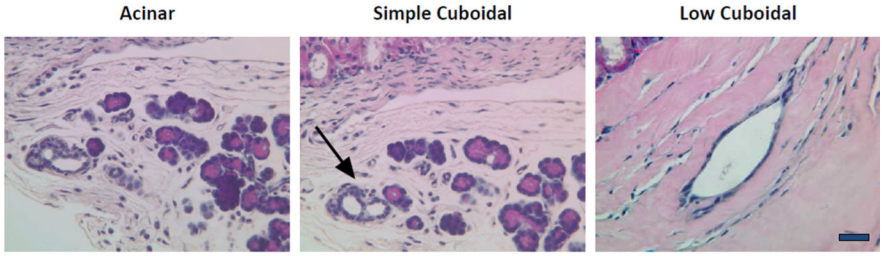

C

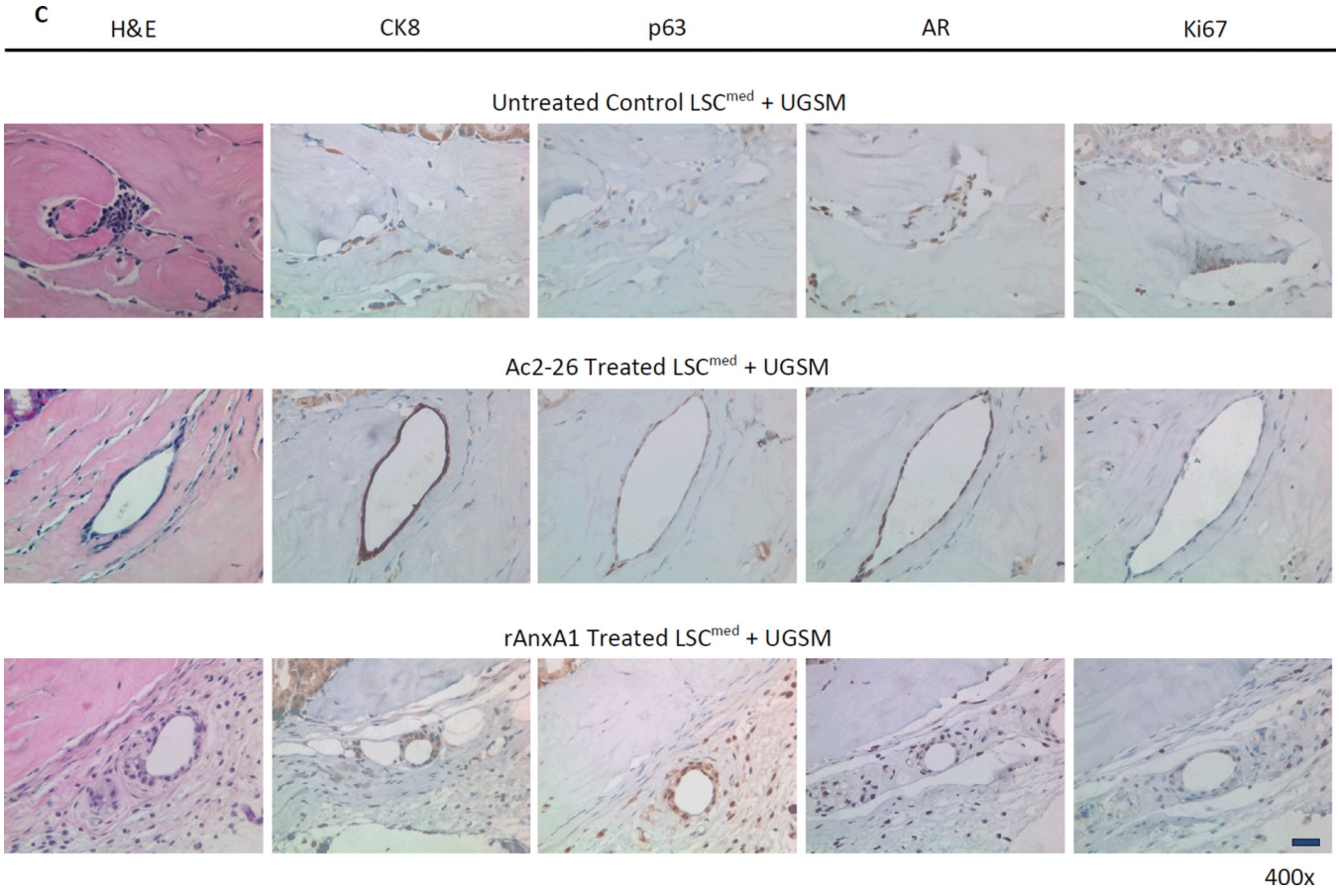

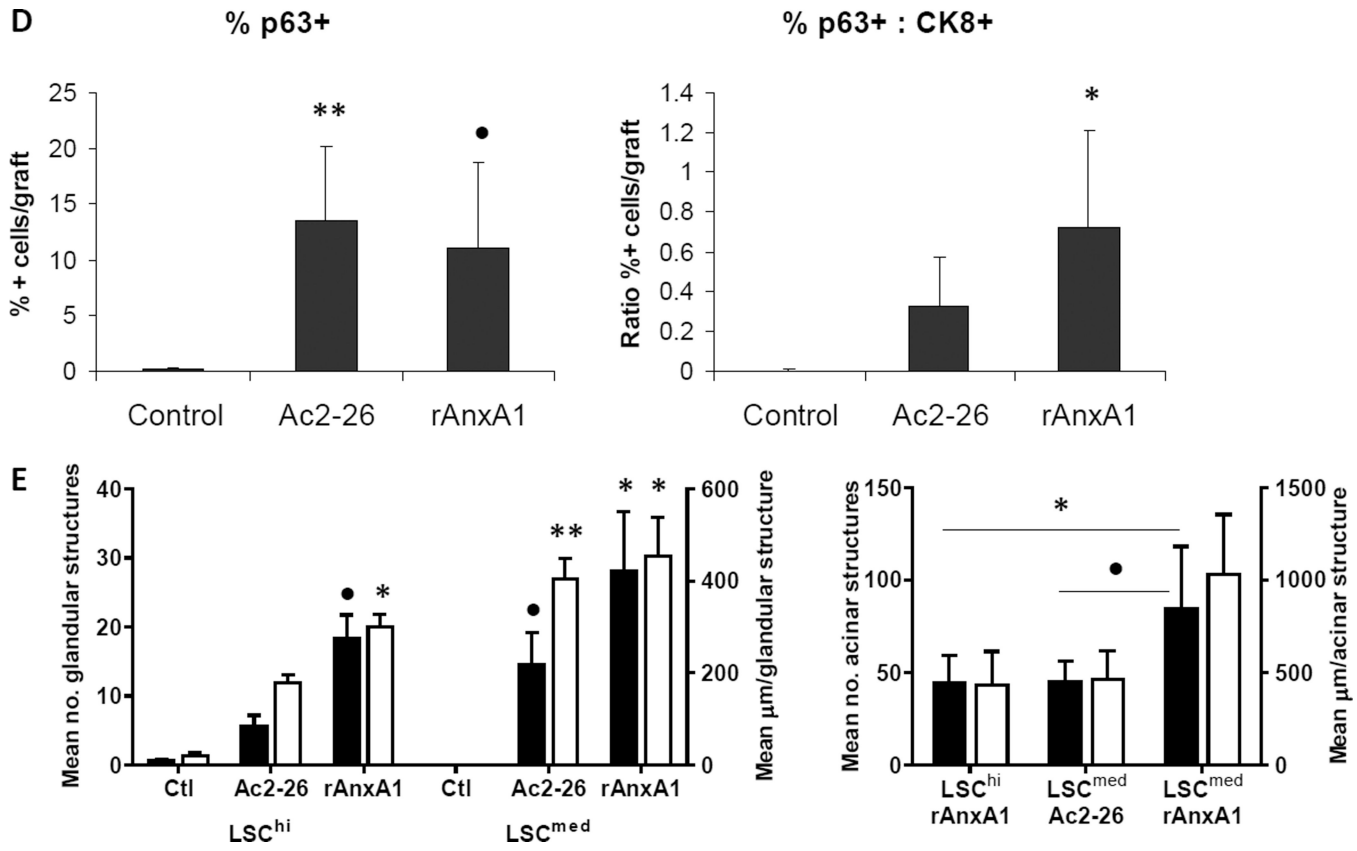

Figure 6.

Effect of AnxA1 on incidence, types, differentiation and proliferation of glandular structures in LSC^{med} grafts (A–D). A, Chart depicting the incidence and type of glandular structures (prostatic glandular or acinar) scored in LSC^{med} untreated control, Ac2-26 treated and rAnxA1 treated grafts. B, Representative H&E images of the types of structures detected in rAnxA1 treated grafts. Black arrow indicates simple cuboidal structure. Magnification at 400×. Bar 100 µm. C, Tissue sections were analyzed by H&E for basic histology and IHC for expression of p63, CK8, AR and Ki67. Magnification at 400×. Bar 100 µm. D, Calculated percentage of p63^{+} cells and ratio of p63^{+} to CK8^{+} cells detected in the grafts. Potential to undergo de-differentiation in response to AnxA1 was assessed by increase in p63 expression compared to CK8. E, AnxA1 treated LSC$^{hi/med}$ form more and larger glandular structures than controls. rAnxA1 treated LSC^{med} form more and larger acinar glandular structures than rAnxA1 treated LSC^{hi} and Ac2-26 treated LSC^{med} cells. Black bars represent left y-axis data and white bars represent right y-axis data. Statistical significance is indicated by *, $P < 0.05$; •, $P < 0.01$; **, $P < 0.001$.

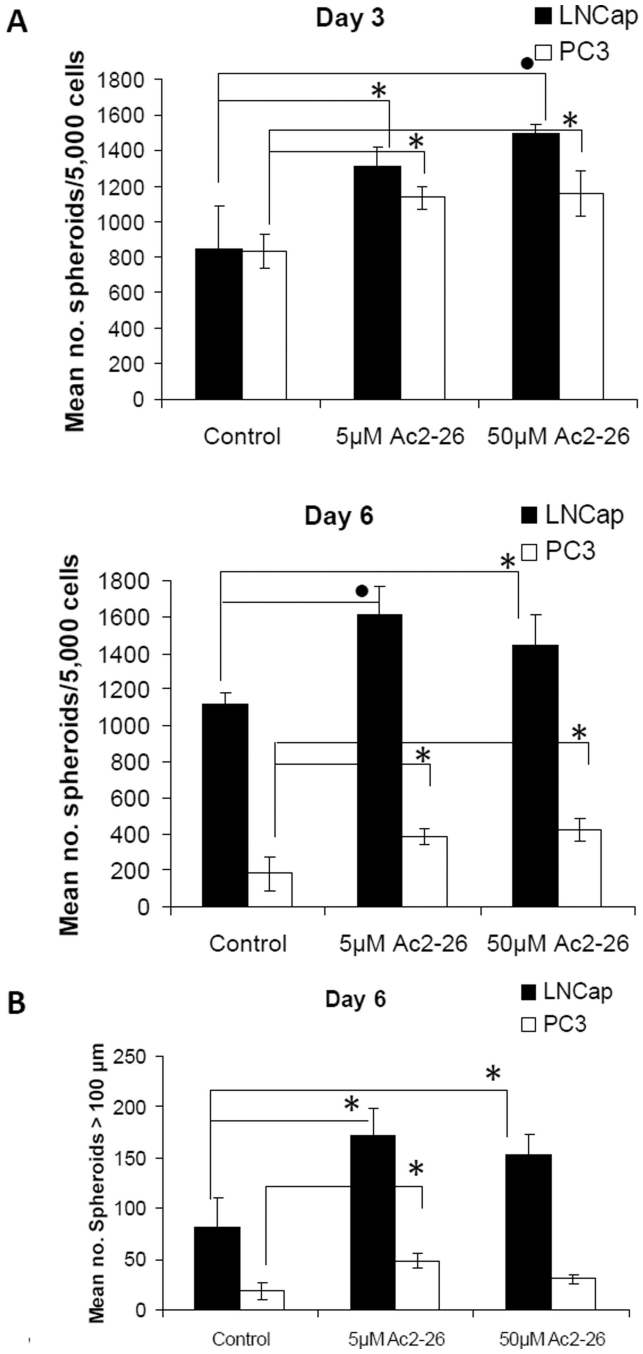

Figure 7.

Effect of AnxA1 mimetic peptide on spheroid formation in human prostate cancer cell lines. A, Spheroids were counted from LNCaP and PC3 human prostate cancer cells grown in 2% Matrigel/2% FBS/RPMI 1640 with treatment on Matrigel pre-coated wells of a 24-well plate at 3 and 6 days after plating. Cells were treated with vehicle control, 5 μM or 50 μM peptide Ac2-26. Mimetic peptide Ac2-26 treatment of LNCaP and PC3 cells led to increased numbers of spheroids formed, at both days 3 and 6, in a non-dose-dependent manner. B, The number of spheroids greater than 100 μm for all culture conditions was counted at day 6.

Representative experiments are shown, and values represent the means ± SD of triplicate samples. Statistical significance is indicated by *, $P < 0.05$; •, $P < 0.01$.